The Astrophysical Journal, 746:38 (6pp), 2012 February 10 doi:10.1088/0004-637X/746/1/38

MATTER DISTRIBUTION AROUND GALAXIES

Shogo Masaki[1], Masataka Fukugita[2,3,4], and Naoki Yoshida[4]
[1] Department of Physics, Nagoya University, Chikusa, Nagoya 464-8602, Japan; shogo.masaki@nagoya-u.jp
[2] Institute for Advanced Study, Princeton, NJ 08540, USA
[3] Institute for Cosmic Ray Research, University of Tokyo, Kashiwa 277-8582, Japan
[4] Institute for the Physics and Mathematics of the Universe, University of Tokyo, Kashiwa 277-8583, Japan
Received 2011 May 13; accepted 2011 November 14; published 2012 January 23

ABSTRACT

We explore the mass distribution of material associated with galaxies from the observation of gravitational weak lensing for the galaxy mass correlation function with the aid of *N*-body simulations of dark matter. The latter is employed to unfold various contributions to the integrated line-of-sight mass density. We conclude that galaxies have no definite edges of the matter distribution, extending to the middle of neighboring galaxies with the density profile roughly $r^{-2.4}$ beyond the virial radius. The mass distributed beyond the virial radius (gravitationally bound radius) explains the gap seen in the mass density estimates, the global value $\Omega_m \sim 0.27$ and typically $\Omega_{\rm gal} \sim 0.15$ from the luminosity density multiplied by the mass-to-light ratio. We suggest using a physical method of gravitational lensing to characterize galaxy samples rather than characterizing them by photometric means.

Key words: dark matter – galaxies: halos – gravitational lensing: weak – large-scale structure of universe

Online-only material: color figures

1. INTRODUCTION

Where and how matter is distributed in the universe is a long-standing question. The widely accepted view is that matter in the universe is preponderantly borne by galaxies. This leads to an estimate of the mass density of the universe (Ostriker et al. 1974). With modern parameters, the luminosity density $\mathcal{L} = 2.2 \pm 0.3 \times 10^8\, h\, L_\odot\, {\rm Mpc}^{-3}$ (Blanton et al. 2001, 2003) multiplied by the average mass-to-light ratio of galaxies, $\langle M/L\rangle \approx (170 \pm 50)\, h\, M_\odot/L_{r\odot}$, from the gravitational lensing shear around 2×10^4 galaxies (McKay et al. 2001) leads to the mass density of the universe $\rho_m = \mathcal{L} \times \langle M/L\rangle$ as

$$\Omega_m = 0.13 \pm 0.05 \tag{1}$$

in units of the critical mass density. The mass of M/L we adopted here is supposed to represent the virial mass, i.e., the mass of particles gravitationally bound in galaxies. This M/L is consistent among a number of estimates for individual galaxies (e.g., Bahcall & Fan 1998).

On the other hand, we now have a convincing estimate of the global matter density from the cosmic microwave background radiation anisotropy (Komatsu et al. 2011), which converges to

$$\Omega_m = 0.27 \pm 0.03. \tag{2}$$

The difference between Equations (1) and (2) raises the problem as to where the missing matter is, indicated by the mismatch of the two numbers.

Within the bound radius of galaxies, the mass distribution is inferred to obey a profile close to that advocated by Navarro et al. (1997, hereafter NFW) in the cold dark matter (CDM)-dominated universe. Simulations of clustering of dark matter conveniently point toward this distribution for mass assemblies. This is also supported by gravitational lensing analysis for bright galaxies (Mandelbaum et al. 2006). Little is studied, however, concerning the mass distribution beyond the virial radius.

Observational advancement with large galaxy samples renders gravitational weak lensing a powerful tool to explore the average surface mass density of galaxies. The measure is the surface density $\Sigma(R)$ as a function of the projected radius from the center of the galaxy R,

$$\Sigma(R) = \int \rho\big(r = \sqrt{R^2 + \chi^2}\big) d\chi, \tag{3}$$

where ρ is the density at r and χ is the line-of-sight distance, both measured from the center of the galaxy. This quantity can be explored along the line of sight toward a light source by measuring its tangential shear $\gamma_{\rm t}$ or magnification μ of the image of background sources, as

$$\gamma_{\rm t}(R) = \frac{\bar{\Sigma}(<R) - \Sigma(R)}{\Sigma_{\rm cr}} = \frac{\Delta\Sigma(R)}{\Sigma_{\rm cr}}, \tag{4}$$

$$\mu(R) \simeq 1 + 2\kappa(R) = 1 + 2\frac{\Sigma(R)}{\Sigma_{\rm cr}}, \tag{5}$$

where $\bar{\Sigma}(<R)$ is the average of Σ within R, κ is the convergence, and $\Sigma_{\rm cr} = (c^2/4\pi G)(D_s/D_{\ell s} D_\ell)$ is the critical surface density.[5] With large modern samples this is applicable even to the outskirts of galaxies significantly beyond the virial radius, say, to $\sim 10\, h^{-1}$ Mpc using either lensing shear (Sheldon et al. 2004; Mandelbaum et al. 2006; Reyes et al. 2010) or statistical magnification (Ménard et al. 2010, hereafter MSFR). While $\Sigma(R)$ thus obtained includes the surface mass density from neighboring galaxies along the line of sight, this quantity gives cogent evidence of the surface mass density profile of the galaxy away from its central region.

MSFR have shown that $\Sigma(R)$ decreases approximately as $R^{-\beta}$ with $\beta = 1 \pm 0.2$ to $R < 1\, h^{-1}$ Mpc, which somewhat flattens to $\beta = 0.6 \pm 0.4$ beyond $R \approx 1$–$10\, h^{-1}$ Mpc using galaxy samples of the Sloan Digital Sky Survey (SDSS; York et al.

[5] Equation (5) is the Taylor expansion to the first order in distortion. Ménard et al. (2003) examined the accuracy of the formula with the conclusion that the higher-order terms contribute about 10%–15% to magnification.

2000; Abazajian et al. 2005). They used the correlation of the magnification signal of background quasars with foreground galaxies. They also showed that the surface density profile derived from the magnification agrees with that from the tangential shear of galaxies (Sheldon et al. 2004). Mandelbaum et al. (2006) have also derived the surface mass density profile for the luminous red galaxy (LRG) sample, which lies parallel to that of MSFR for $R < 1\,h^{-1}$ Mpc, but with their amplitudes about 2.5 times larger than that of MSFR. The difference of the surface mass density of the two profiles diminishes with distance, and the two agree at $R > 1\,h^{-1}$ Mpc, albeit with substantial errors in the measurements.

In this paper, we study the distribution of matter around galaxies with the aid of an extensive use of *N*-body simulations for the CDM-dominated universe without baryons, which have been convergent among different simulations to a sufficient accuracy. We employ *N*-body simulations to unfold contributions from multiple galaxies and to interpret the finding from gravitational lensing, but also to extrapolate the physics to the region beyond the reach of the observation after verifying that the *N*-body simulation indeed describes the observed surface mass density profile with an accuracy sufficient for us. We note that Hayashi & White (2008) also used large numerical simulations to study the dependence of the galaxy/halo-matter cross-correlation amplitude on the galaxy mass and the halo mass. We expect that the state-of-the-art *N*-body simulation for dark matter gives information that is sufficiently reliable for the quantity where the observations would not directly give the information, if the simulation is appropriately constrained by the observation. This gives insight into the distribution of the matter beyond the observation and would reveal a more global distribution of matter in the universe considerably away from galaxies.

In Section 2, we describe the *N*-body simulation. In Section 3, we present the surface mass density profile in reference to the observation. In Section 4 we discuss the mass distribution beyond the virial radius and note that caution is necessary regarding the aperture when the mass of galaxies is referenced. Section 5 is a summary of our analysis.

2. COSMOLOGICAL *N*-BODY SIMULATIONS

We use the parallelized *N*-body simulation code *Gadget-2* (Springel et al. 2001; Springel 2005) in its Tree-PM mode. Baryons are not included. We assume a flat universe with cosmological parameters $\Omega_m = 0.258$ and $h = 0.719$, the Hubble constant in units of $100\,\mathrm{km\,s^{-1}\,Mpc^{-1}}$; for other parameters $n_s = 0.963$ and $\sigma_8 = 0.796$, following the parameters derived in the *WMAP* five-year result (Komatsu et al. 2009). The gravitational softening parameter is chosen to be $\epsilon = 10\,h^{-1}$ kpc. We take 1024^3 particles in a box of comoving $200\,h^{-1}$ Mpc on a side. The mass of a dark matter particle is $5.34 \times 10^8\,h^{-1}\,M_\odot$, so that we are able to identify halos with mass a few times $10^{10}\,h^{-1}\,M_\odot$. We set the initial redshift at $z_i = 50$ and generate the initial condition using the second-order Lagrangian perturbation theory[6] (Scoccimarro 1998), which has the advantage that it is more accurate in generating initial conditions so that one can set them at an epoch later than with the conventional Zeldovich approximation; see Crocce et al. (2006) and Jenkins (2010). The initial matter power spectrum at $z = z_i$ is computed using the *CAMB* code (Lewis et al. 2000).

[6] The parallelized second-order Lagrangian perturbation theory code (Nishimichi et al. 2009) is provided by T. Nishimichi.

Table 1
Halos Identified in Our Simulation at $z = 0.36$

Mass ($h^{-1}\,M_\odot$)	Number	Number Fraction (%)	Mass Fraction (%)
5×10^{10}–5×10^{11}	189,578	82.5	5.9
5×10^{11}–5×10^{12}	36,402	15.8	8.25
5×10^{12}–5×10^{13}	3,637	1.6	7.64
5×10^{13}–5×10^{14}	187	0.08	3.13

Halos are identified in two steps. We select candidate groups of dark matter particles using the friends-of-friends algorithm, where we take the linking length to be $b = 0.2$. We then apply the spherical overdensity algorithm to the candidate groups that are identified by friends of friends. We choose groups that contain at least 100 particles. We follow the conventional operational definition for the pseudovirial radius (r_v): when the particles enclosed within some radius give the average mass density $200 \times \rho_{\rm crit}(z)$, they form a halo, the mass of which is given by the sum of those particles and is referred to as the virial mass M_v. Taking the minimum number of particles in a halo to be 100, i.e., the minimum mass of the halo is $5.3 \times 10^{10}\,h^{-1}\,M_\odot$, we identify 229,804 halos. Table 1 shows the number of halos we identified in the simulation at $z = 0.36$, which is the average redshift of the galaxy sample used by MSFR.

We confirmed that the halo mass function agrees with modern simulations to good accuracy, e.g., with that by Crocce et al. (2010), but also with the analytic formula of Sheth & Tormen (1999) with a known slight deviation as reported by the above reference. We fit all groups with the NFW profile and compare the concentration parameter $c = r_{\rm vir}/r_s$ (r_s is the scale length of the NFW profile) as a function of halo mass with other modern simulations. We confirmed that our c agrees with that of Macciò et al. (2008; see also Bullock et al. 2001) within a few percent level. The simulations are well converged, and the difference in simulations and analysis algorithms is tolerably small.

The scale range of concern in this paper is $20\,h^{-1}$ kpc or larger, where the contribution from baryons little modifies the surface mass density profile. Hence, we confine ourselves to the CDM universe without baryons.

3. SURFACE MASS DENSITY PROFILES AROUND HALOS

We calculate the mean surface mass density around halos in the following way. We shift the entire box so that it is centered on the halo being considered. We consider a beam and project the mass of simulation particles within comoving $100\,h^{-1}$ Mpc widths to the beam. This gives the surface mass density around the beam at a specific projected distance. We then take the average of the beams around all halos to obtain the projected surface mass density profile.

Figure 1 compares our simulation for the surface mass density at $z = 0.36$ with the observational result of MSFR, which was derived at the same mean redshift. The abscissa is the physical distance at this redshift from the center of the halo. The simulation is represented by a bunch of thin curves for 100 halos randomly chosen from the 9970 halos that have a virial mass larger than $2 \times 10^{12}\,h^{-1}\,M_\odot$ (this choice is discussed below). The maximum halo mass in our simulation is $5 \times 10^{14}\,h^{-1}\,M_\odot$. The thick solid curve is the average over the entire sample above the mass threshold. The observational data (ticks with error bars) are taken from MSFR. The simulation agrees with

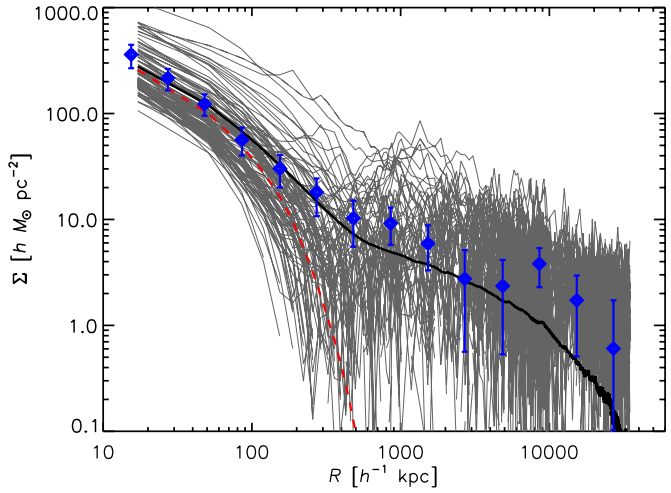

Figure 1. Surface mass density profile as a function of the distance from the center of galaxies. The bunch of thin solid curves represents the profiles for 100 randomly selected halos from 9970 halos with mass $\geqslant 2 \times 10^{12}\, h^{-1}\, M_\odot$ generated in the ΛCDM *N*-body simulation. The thick solid curve is the mean of all halos above the mass threshold. The dashed curve shows the contribution from the one-halo term. The data with error bars are the observational estimate using the galaxy mass correlation function deduced from gravitational weak lensing for quasar brightness in MSFR. The abscissa is the physical distance at $z = 0.36$, which is the average redshift of the weak lensing observation.

(A color version of this figure is available in the online journal.)

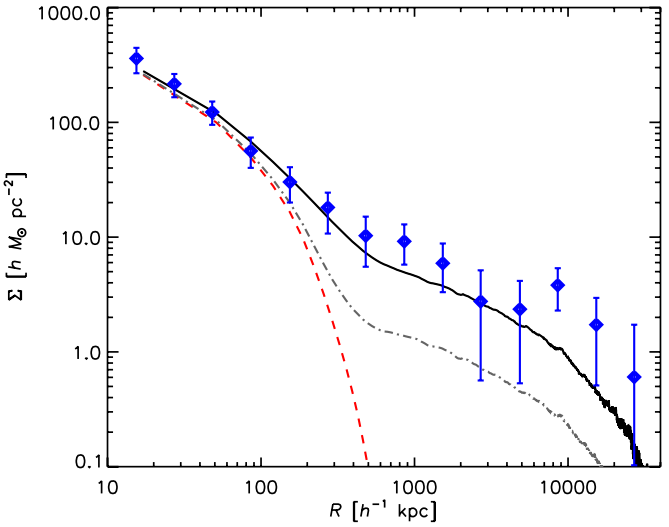

Figure 2. Mean surface mass density profile as a function of the distance from the center of galaxies. The thick solid curve is the mean of all halos above the mass threshold. The dash-dotted curve represents the contribution from particles bound to halos, i.e., particles that reside within the virial radius of all halos. The data with error bars are the observational estimate by MSFR as in the previous figure.

(A color version of this figure is available in the online journal.)

the observation very well, in both overall shape and amplitude up to $10\, h^{-1}$ Mpc.

The dashed curve shows the contribution from the central halos, which are truncated at their virial radii, the so-called one-halo term. The figure shows that the mean surface density at $R \lesssim 200\, h^{-1}$ kpc is dominated by the one-halo term. We note that our column integrates over all particles along the line of sight and would receive a contribution not only from the tail of neighboring halos but also from possible "unbound" particles away from galaxies.

To separate the contributions of bound and unbound particles, we remove the particles beyond the virial radii of all halos. Then we recompute the surface mass density in the same way as described above, but including halos with mass below our virial mass threshold set above. This is shown in Figure 2 with the dash-dotted curve, which stands for the contributions from bound particles in all halos. The data, the thick solid and the dashed curves, are the same as in Figure 1. The figure shows a substantial difference between the solid and dash-dotted curves, meaning that particles bound in halos contribute only 1/3 the total surface mass density beyond a distance of $\approx 500\, h^{-1}$ kpc from the galaxy. We recall that the total surface mass density derived in the simulation agrees with that estimated from gravitational lensing. Roughly 2/3 of the surface mass density at such a distance is due to particles residing beyond the virial radius of any galaxies, i.e., gravitationally "unbound" particles.

In our argument we set the cutoff on the lowest mass of halos, somewhat arbitrarily, at $2 \times 10^{12}\, h^{-1}\, M_\odot$. This choice should of course affect the surface mass density profile. We show in Figure 3 the mass density profiles with different threshold mass: 5×10^{11}, 2×10^{12}, 5×10^{12}, 2×10^{13}, and $5 \times 10^{13}\, h^{-1}\, M_\odot$. We see that the surface mass density increases as the lower cutoff mass (virial mass) $M_{\rm low}$ increases for small radii, say, $R < 1\, h^{-1}$ Mpc where the one-halo term is the significant contributor. The result of the simulation shows $\Sigma(R) \propto M_{\rm low}^{2/3}$ for a distance scale of 10 kpc to a few hundred kpc: it is summarized, e.g., at $120\, h^{-1}$ kpc as

$$\Sigma \simeq 100 (M_{\rm low}/8 \times 10^{12}\, h^{-1}\, M_\odot)^{2/3}\, h\, M_\odot ({\rm pc})^{-2}. \quad (6)$$

With the singular isothermal sphere we have the surface mass density at the projected distance R,

$$\Sigma(R) = \left(\frac{25\pi}{6}\rho_{\rm crit}\right)^{1/3} M_v^{2/3}\frac{1}{R}, \quad (7)$$

and a similar relation holds with the NFW profile albeit in the limited distance range. With our mass function the average mass $\langle M_v \rangle \approx 5 M_{\rm low}$, so that our fitting formula (Equation (6)) gives for a given $\Sigma(R)$ a halo mass 2.5 times smaller than the model with the singular isothermal sphere.

This sample threshold dependence explains the difference in the surface mass density distributions of Mandelbaum et al. (2006), also plotted in Figure 3, and of MSFR. The former gives $\Sigma(R)$ larger by a factor of 2.5 than MSFR within a few hundred kpc range. Equation (6) then indicates that the threshold mass of the LRG sample of Mandelbaum et al. (2006) is approximately four times that of MSFR, who used the main galaxy sample. The difference seen in $\Sigma(R)$ among different halo masses diminishes for large R, where the one-halo term no longer dominates but $\Sigma(R)$ is contributed by neighboring halos and unbound particles, as seen by comparing $\Sigma(R)$ of Mandelbaum et al. (2006) and MSFR.[7] (Neighboring halos are more likely to be those of normal galaxies rather than LRGs.)

Figure 3 indicates that the mean surface mass density profile around galaxies measured by MSFR is well reproduced when the threshold mass $M_{\rm low}$ is set to $2 \times 10^{12}\, h^{-1}\, M_\odot$, which is approximately the mass of the L^* galaxy, $1.2 \times 10^{12}\, h^{-1}\, M_\odot$ (Fukugita & Peebles 2006); hence, our default cutoff is chosen.

[7] The LRG data show a slightly larger amplitude at $R \sim 1\, h^{-1}$ Mpc, reflecting greater bias. The overall features of the surface density profiles for different galaxy/halo masses are studied in detail by Hayashi & White (2008).

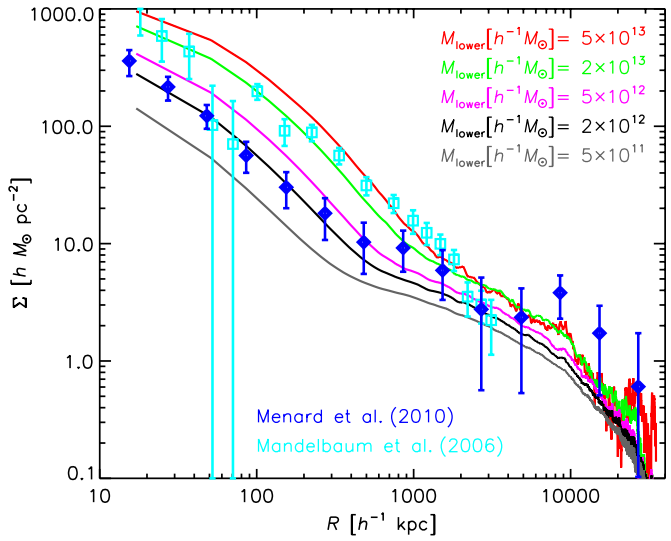

Figure 3. Mean surface mass density profile as a function of the distance from the center of galaxies for galaxy samples with different threshold halo mass (virial mass). The open squares, which represent the data for LRGs given by Mandelbaum et al. (2006), are added to the MSFR data for the SDSS main galaxy sample, shown as solid diamonds with error bars.

MSFR used the galaxy sample $17 < i < 21$. If the effective cutoff of the sample is around $i \approx 20$, the sample's threshold is around the L^* galaxy[8] (Blanton et al. 2001).

It is less ambiguous to estimate the threshold mass from $\Sigma(R)$ itself. With the threshold $2 \times 10^{12}\, h^{-1}\, M_\odot$, $\Sigma(R)$ of the simulation is in good agreement with the data. If we were to take the threshold $5 \times 10^{11}\, h^{-1}\, M_\odot$, which roughly corresponds to the $i \approx 21$ mag threshold, $\Sigma(R)$ of the simulation would lie somewhat too low. This consideration suggests that the surface mass density can be used to characterize the mass of the galaxy sample, which otherwise is difficult to estimate accurately.

In the limited range of the distance scale we are studying, $15\,\mathrm{kpc} < R < 200\,\mathrm{kpc}$, both NFW and singular isothermal sphere give mass profiles that are very similar, and both give good fits to the data, so that we are not able to distinguish between the two profiles in this range.

4. MASS DISTRIBUTION BEYOND THE VIRIAL RADIUS

We see above that a substantial amount of matter in the universe resides outside the pseudovirial radius of galaxies. In order to examine whether the distribution of unbound particles is organized, we calculate the total amount of mass encircled with the pseudovirial radius and then expand the encircling radius by a factor of α: we denote it in units of the critical density as $\Omega_{\rm halo\ extended}(\alpha)$. The pseudovirial radius is defined for each galaxy as 200 times $\rho_{\rm crit}$. For large α two halos start overlapping, and in such cases we count the amount of material only once, avoiding double counting. Figure 4 shows the fraction $\Omega_{\rm halo\ extended}(\alpha)/\Omega_m$ as a function of α, which is described well with $0.23 \ln\alpha + 0.22$, consistent with the NFW profile in its $\rho \sim r^{-3}$ regime.

If the mass distribution of a galaxy were spatially bounded, it would not matter what encircling radius is used for the mass estimate of galaxies, as long as it was large enough. We find, however, that this is not the case. The encircling radius must be carefully specified, for instance, to calculate the mass-to-light ratio to be quantitatively meaningful.

The figure shows that the matter within the pseudovirial radius ($\alpha = 1$) is only 0.25 times the total matter if the sample of galaxies is set above the mass threshold $10^{11}\, h^{-1}\, M_\odot$, above which the galaxy mass (and hence M/L) is observationally estimated; see below. This fraction (and the curve in the figure) depends on the threshold mass of sample galaxies, as $\sim -\log M_{\rm low}$ insofar as $M_{\rm low}$ is taken below the break mass of the mass function. If the threshold is taken at a larger mass, this fraction decreases faster, mainly because the number of galaxies included in the sample decreases. Note that the sample threshold must be taken small enough to estimate the mass density of the universe so that the contribution of subthreshold galaxies to the global quantity (in practice, luminosity density) is not substantial. We confirm that this mass fraction agrees with the mass obtained by integrating over the mass function. The figure also shows that this fraction becomes close to 0.5 if three times the pseudovirial radius is taken to encircle clustering. Almost all matter (>90%) is included only with $\alpha > 20$.

Now it may be appropriate to examine the case discussed by McKay et al. (2001), who estimated the mass of galaxies from gravitational lensing shear, as we quoted earlier. They used the spectroscopic sample of the SDSS, which means the limiting magnitude accurately defined at $r_{\rm limit} = 17.8$ (Strauss et al. 2002). It corresponds to $M_r \approx -20.6$ for the median redshift of the sample $z \approx 0.10$ with the median K correction, or to $0.41 L_r^*$. If we invoke an empirical scaling relation $M \propto L^2$ (Mandelbaum et al. 2006) as consistent with the Faber–Jackson relation, we estimate the limiting mass of the sample $M_{\rm low} \approx 2 \times 10^{11}\, h^{-1}\, M_\odot$, taking $M_{\rm MW} \approx 2.3 \times 10^{12}\, M_\odot$ (Fukugita & Peebles 2006) and $L_{\rm MW} = 1.4\, L_*$ for the Milky Way to normalize the M–L relation.

This can also be verified from the gravitational lensing measurement itself. McKay et al. (2001) obtained $\Sigma(R) \approx 2.5(R/1\, h^{-1}\,\mathrm{Mpc})^{-0.8\pm0.2}\, h\, M_\odot\,\mathrm{pc}^{-2}$. Consulting with our $\Sigma(R)$ relation with the sample threshold mass as a parameter (see Figure 3), we estimate $M_{\rm low} \approx 1.5 \times 10^{11}\, h^{-1}\, M_\odot$, in agreement with the photometric estimate.

With this threshold, we estimate a mean virial mass of the spectroscopic sample of $\overline{M}_v \approx 1.5 \times 10^{12}\, h^{-1}\, M_\odot$ using the mass function obtained in our simulation. This value is compared with the estimate $\overline{M}_v \approx (2.6 \pm 1.3) \times 10^{12}\, h^{-1}\, M_\odot$ of McKay et al. (2001) for their sample, where the error includes the variance associated with the galaxy morphology. This shows the consistency of the two estimates: those by McKay et al. (2001) and ours.

Our simulation gives the average pseudovirial radius over the sample with the lower mass cutoff $M_{\rm low}$ as $\overline{r}_v = 100\, h^{-1}\,\mathrm{kpc}(M_{\rm low}/10^{11}\, h^{-1}\, M_\odot)^{0.29}$, so that our estimate of the virial radius $\overline{r_v}$ for the sample with $M_{\rm low} \approx 1.5 \times 10^{11}\, h^{-1}\, M_\odot$ is $\overline{r}_v = 120\, h^{-1}\,\mathrm{kpc}$. McKay et al. (2001) claim that they measured the M/L within $260\, h^{-1}\,\mathrm{kpc}$, which is $\alpha \approx 2.2$ times the mean virial radius of the sample. Figure 4 tells us that for $\alpha = 2.2$ approximately 0.4 times the total Ω_m should be included in their estimate. This leads us to a global matter density from galaxies of

$$\Omega_m = (0.13 \pm 0.05)/0.4 \approx 0.32, \qquad (8)$$

which is consistent with the global value of Equation (2). Although our estimate presented here is admittedly crude, this agreement indicates that the mass beyond the pseudovirial radius we inferred here is probably broadly correct. We should

[8] At a more accurate level we must consider that L^* luminosity corresponds to $10^{10.6}\, L_\odot$ in the i band but to $10^{10.5}\, L_\odot$ in the r band. L^* luminosity is not physically well defined. We also note that there is a significant uncertainty in the mass–luminosity relation associated with the morphology of galaxies.

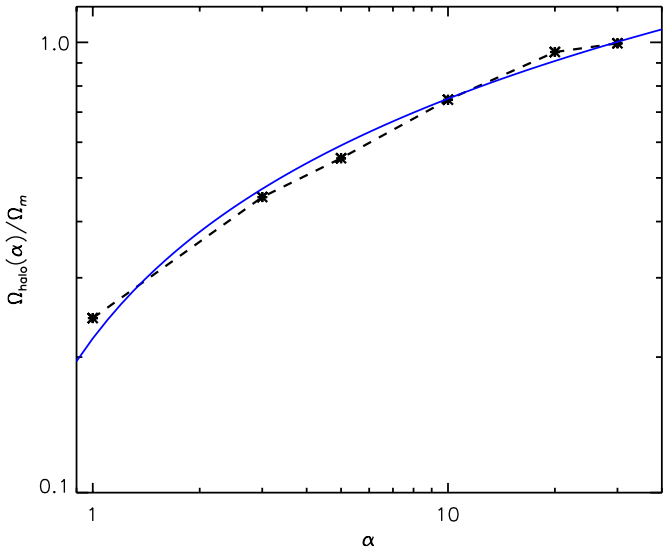

Figure 4. Fraction of mass contained in the sphere centered on individual halos with radius $\alpha R_{\rm vir}$, where $R_{\rm vir}$ is the pseudovirial radius and α is the multiplier represented in the abscissa. The plot is for the sample with the threshold halo mass $1 \times 10^{11}\,M_\odot$. The solid curve is $0.23 \ln\alpha + 0.22$ given in the text.
(A color version of this figure is available in the online journal.)

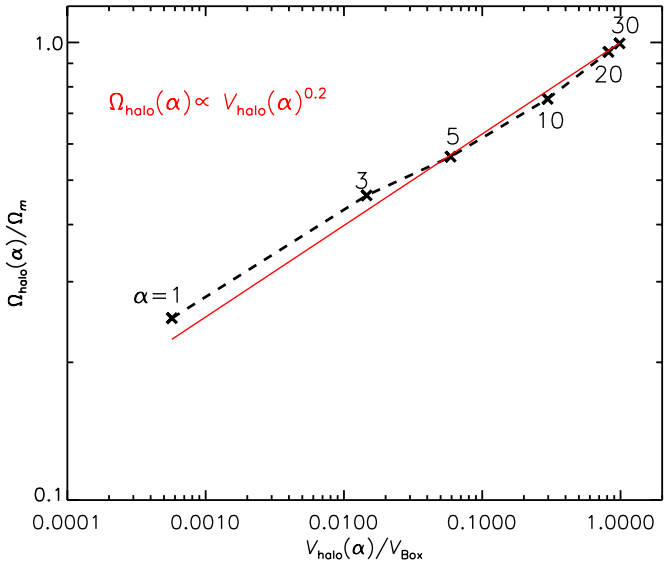

Figure 5. Mass fraction borne by extended halos with the radius $r \leqslant \alpha R_{\rm vir}$, $\Omega_{\rm halo\ extension}(\alpha)/\Omega_m$ vs. the volume fraction occupied by the extension of virial spheres $V_{\rm halo\ extension}(\alpha)/V_{\rm tot}$. The numbers shown beside the symbol are the multiplier α. The solid line indicates $\Omega_{\rm halo\ extension}/\Omega_m \sim (V_{\rm halo\ extension}/V_{\rm tot})^{0.2}$.
(A color version of this figure is available in the online journal.)

underline the importance of the estimate of the radius (e.g., with respect to the virial radius) when the mass or the mass-to-light ratio is presented for galaxies, since galaxies are extended objects without definite boundaries.

We next calculate the volume occupied with extended halos as a function of α. In Figure 5, we plot the fraction of mass contained in the extension of halos $\Omega_{\rm halo\ extension}(\alpha)/\Omega_m$ as a function of the fraction of the volume occupancy $V_{\rm halo\ extension}(\alpha)/V_{\rm total}$, where $V_{\rm total}$ is the total simulation volume. The numbers beside the symbol indicate the multiplier α. $V_{\rm halo\ extension}$ is approximately proportional to $(\alpha R)^3$ up to overlaps of halos at a large α. This figure shows that the plot is given nearly by a straight line, indicating that

$$\Omega_{\rm halo\ extension}(\alpha)/\Omega_m \sim [V_{\rm halo\ extension}(\alpha)/V_{\rm total}]^{0.2}. \quad (9)$$

Let us recall that if the mass distribution is random throughout the entire volume, we expect $\Omega_{\rm halo\ extension} \propto V_{\rm halo\ extension}$. The figure shows that there is no symptom of a conspicuous break of the curve at any α, meaning that the distribution of unbound matter is all organized to a distance significantly away from the galaxy, without leaving a significant amount of material in the intergalactic space. This power means that the matter density behaves as

$$\rho_m \sim r^{-2.4} \quad (10)$$

beyond the virial radius, as long as halfway to the neighboring galaxy. This drops faster than the isothermal profile but is numerically consistent with the tail of the NFW profile in the range $r/r_s = 5$–100, with r_s the NFW scale radius. Remembering that $r_v/r_s \approx 5$ for galaxies and the typical spacing between the galaxies is $r_0 \approx 5\,h^{-1}$ Mpc, the relevant range matches the inter-galaxy distance.

Since galaxies have no clear edges, it is not appropriate to define their "total" mass. If we include the mass in the tail of the galaxy halfway to the neighboring galaxy, the mass of the galaxy increases approximately by a factor of two so that the effective M/L becomes $\approx 350\,h\,M_\odot\,L_\odot^{-1}$. When multiplied by the luminosity density $\mathcal{L} = 2.2 \times 10^8 h\,L_\odot\,{\rm Mpc}^{-3}$, we obtain

$$\rho_m = \mathcal{L} \times \langle M/L \rangle \approx 0.3\rho_{\rm crit}, \Omega_m \approx 0.3. \quad (11)$$

We remark that clusters serve as a good natural integrator of the mass of galaxies. The mass of clusters is usually estimated at the radius, say, r_{500}, which is far beyond the virial radii of individual member galaxies. Therefore, the mass of galaxies residing in the tail is largely integrated in the estimate of the cluster mass. This explains why M/L of clusters reaches 300–400, significantly larger than the estimates for individual galaxies: the mass here includes the mass present in the tail of galaxies. This explains why we arrived at the correct global mass density of the universe if the *cluster* M/L is multiplied by the luminosity density of *field* galaxies instead of the M/L of individual galaxies, though this is apparently an incongruous treatment.

5. SUMMARY

We showed that the state-of-the-art N-body simulation of dark matter based on the ΛCDM model gives an excellent description of the surface density profile of the mass distribution around galaxies, which has been explored up to the $10\,h^{-1}$ Mpc scale from the galaxy mass correlation function using weak gravitational lensing analysis applied to large modern galaxy samples. The surface profile thus derived is consistent with $r^{-1\pm0.2}$ up to $1\,h^{-1}$ Mpc and somewhat flattens to $r^{-0.6\pm0.4}$ beyond this radius. The latter power is consistent with that of the two-point correlation function of galaxies. The galaxy mass correlation function measures the mass distribution within the galaxy halo in a short distance scale (smaller than a few × 100 kpc scale) and reflects the galaxy distribution beyond this radius. The two distributions are similar and match each other with a slight break.

The amplitude of the surface mass density profile depends on the galaxy sample, in particular on the lower mass cutoff applied to the sample. Hence, the amplitude allows us to infer the properties of the galaxy sample in a self-consistent way.

We showed that the galaxy has no clear edges in the dark matter distribution, unlike luminous matter, which should be bounded by the cooling radius. The distribution is extended beyond the virial radius in an organized way halfway to the

neighboring galaxy, so that the universe is filled with the material associated with tails of galaxies, and we then call the peaks of the matter distribution galaxies. Intergalactic space is filled with matter. Tails of galaxies extend to great distances without cutoff, whereas the luminous component of galaxies has a definite cutoff radius corresponding to the cooling radius.

About half the matter in the universe is gravitationally unbound at $z \sim 0$. Its distribution, however, is never random or uniform, but is well organized in a way to be consistent with the tail of galaxies with mass density roughly $\rho \sim r^{-2.4}$. Half the matter is present in the tail of galaxies beyond the pseudovirial radius. This explains the gap in the estimate of mass density of the universe between the global value and the value obtained by adding the contributions from matter bound to individual galaxies: with this extended matter distribution the matter entry closes in the mass inventory, which has been left unclosed in Fukugita & Peebles (2004).[9]

The observables derived from gravitational lensing lead us to characterize the sample in terms of the mass with physical means. The agreement between photometrically inferred characteristics and physically derived ones is, if not yet perfect, almost satisfactory. Gravitational lensing can be used to characterize the sample with physical methods.

We thank Brice Ménard, Masamune Oguri, and Rachel Mandelbaum for useful discussions. We appreciate Tomoaki Ishiyama for providing us with data of their *N*-body simulations. This work is supported in Nagoya and in Tokyo in part by the Grants in Aid of the Ministry of Education. M.F. acknowledges the support of the Friends of the Institute in Princeton.

[9] Fukugita & Peebles (2004) consider that 60% of the matter is bound, i.e., within virial radii, and that the other 40% lies outside. Their inference of these numbers uses M/L estimated by McKay et al. (2001), assuming that their encircled radii are sufficiently large as to cover the binding radius, so that the radius used is 2.2 times the virial radius, as we discussed in the text above. In our present estimate 60% must be modified to 40% in the same context, and the bound component, if defined by the pseudovirial radius, is 25%.

REFERENCES

Abazajian, K., Adelman-McCarthy, J. K., Agüeros, M. A., et al. 2005, AJ, 129, 1755
Bahcall, N. A., & Fan, X. 1998, Proc. Natl. Acad. Sci., 95, 5956
Blanton, M. R., Dalcanton, J., Eisenstein, D., et al. 2001, AJ, 121, 2358
Blanton, M. R., Hogg, D. W., Bahcall, N. A., et al. 2003, ApJ, 592, 819
Bullock, J. S., Kolatt, T. S., Sigad, Y., et al. 2001, MNRAS, 321, 559
Crocce, M., Fosalba, P., Castander, F. J., & Gaztañaga, E. 2010, MNRAS, 403, 1353
Crocce, M., Pueblas, S., & Scoccimarro, R. 2006, MNRAS, 373, 369
Fukugita, M., & Peebles, P. J. E. 2004, ApJ, 616, 643
Fukugita, M., & Peebles, P. J. E. 2006, ApJ, 639, 590
Hayashi, E., & White, S. D. M. 2008, MNRAS, 388, 2
Jenkins, A. 2010, MNRAS, 403, 1859
Komatsu, E., Dunkley, J., Nolta, M. R., et al. 2009, ApJS, 180, 330
Komatsu, E., Smith, K. M., Dunkley, J., et al. 2011, ApJS, 192, 18
Lewis, A., Challinor, A., & Lasenby, A. 2000, ApJ, 538, 473
Macciò, A. V., Dutton, A. A., & van den Bosch, F. C. 2008, MNRAS, 391, 1940
Mandelbaum, R., Seljak, U., Cool, R. J., et al. 2006, MNRAS, 372, 758
McKay, T. A., Sheldon, E. S., Racusin, J., et al. 2001, arXiv:astro-ph/0108013
Ménard, B., Hamana, T., Bartelmann, M., & Yoshida, N. 2003, A&A, 403, 817
Ménard, B., Scranton, R., Fukugita, M., & Richards, G. 2010, MNRAS, 405, 1025 (MSFR)
Navarro, J. F., Frenk, C. S., & White, S. D. M. 1997, ApJ, 490, 493 (NFW)
Nishimichi, T., Shirata, A., Taruya, A., et al. 2009, PASJ, 61, 321
Ostriker, J. P., Peebles, P. J. E., & Yahil, A. 1974, ApJ, 193, L1
Reyes, R., Mandelbaum, R., Seljak, U., et al. 2010, Nature, 464, 256
Scoccimarro, R. 1998, MNRAS, 299, 1097
Sheldon, E. S., Johnston, D. E., Frieman, J. A., et al. 2004, AJ, 127, 2544
Sheth, R. K., & Tormen, G. 1999, MNRAS, 308, 119
Springel, V. 2005, MNRAS, 364, 1105
Springel, V., Yoshida, N., & White, S. D. M. 2001, New Astron., 6, 79
Strauss, M. A., Weinberg, D. H., Lupton, R. H., et al. 2002, AJ, 124, 1810
York, D. G., Adelman, J., Anderson, J. E., Jr., et al. 2000, AJ, 120, 1579